3-D Coverage Beam-Scanning Antenna Using Feed Array and Active Frequency-Selective Surface

Chao Gu, Steven Gao, *Senior Member, IEEE*, Benito Sanz-Izquierdo, Edward A. Parker, Fan Qin, Hang Xu, John C. Batchelor, *Senior Member, IEEE*, Xuexia Yang, and Zhiqun Cheng

***Abstract*— This paper presents the design of a smart antenna that can achieve 3-D beam-scanning coverage. The antenna consists of a novel planar feed array and a cylindrical active frequency-selective surface (AFSS). First, an array fed metallic reflector is studied as a reference antenna to validate the beam-scanning characteristics in the elevation plane. Then, the AFSS is assessed through simulation and measurement results. Finally, the complete structure containing the planar collinear array and the AFSS is analyzed. A prototype at S-band has been designed, manufactured, and measured. The resulting antenna is shown to be able to operate at the 2.4–2.5 GHz frequency band and switch beams in both the azimuth and elevation planes. In the azimuth plane, the proposed antenna is capable of sweeping beams toward different directions to cover a full range of 360°. In the elevation plane, it can achieve beam steering within an angle range of $+16°/-15°$. The measured maximum gain of the antenna is 9.2 dBi. This is the first report of a low-cost 3-D coverage beam-scanning antenna based on AFSS.**

***Index Terms*— 3-D beam switching, electronically beam-steering antennas, frequency-selective surface (FSS), reconfigurable antennas, smart antennas.**

I. Introduction

AFTER decades of exponentially growing demands placed on handling the vast amount of wireless data volumes, wireless system design is faced with challenges in spectrum efficiency, cell capacity, and cost-effective deployment. During recent years, smart antennas, e.g., phased arrays or adaptive arrays, are becoming increasingly important for applications in wireless communications as they can offer a significant increase in channel capacity and coverage range. As a conventional solution, however, an adaptive array is expensive, complex, bulky, and power hungry [1]. Thus, it is currently limited to applications in military and defense systems, for example, active electronically steered array radars. The cost and complexity are mainly proportional to the number of array elements that connect to RF/microwave phase shifters, transmit/receive (T/R) modules, and power distribution networks. To facilitate the future 5G applications, it is expected that smart antennas would have a compact size, low power consumption, and are affordable to a larger number of users in contrast to conventional phased arrays. Another design consideration is the beam-scanning coverage. For example, in interbuilding wireless link scenario, it is desirable that smart antennas offer a full 360° angular coverage in the horizontal plane and steerable beams in the elevation plane to provide sufficient signal strength to dynamic users in different levels of the buildings.

As an alternative solution, reconfigurable antennas featuring switchable/tunable frequency/polarization/patterns can be used to increase system diversity level and achievable channel capacity while reducing prohibitive system costs [2], [3]. Similar to conventional smart antennas, pattern reconfigurable (switched beam) antennas have attracted extensive research interest to improve the antenna performance by applying new reconfiguring techniques. For instance, ESPAR antennas proposed in [4], [5] offer a cost-effective implementation, where p-i-n diodes/varactors are loaded at the parasitic antenna array elements instead of using phase shifters to steer radiation patterns in the azimuth plane. In [6], a circular Yagi-Uda array incorporates liquid metal mercury into the director and reflector elements to reconfigure the antenna radiation patterns. Recently, electromagnetic structures such as metamaterials and frequency-selective surfaces (FSSs) have also been engineered to achieve antenna beam switching/steering [7]–[10] thanks to their fabrication simplicity and enhanced reconfigurability using various tuning technologies. Ji *et al.* [11] present a beam steering partially reflective surface antenna fed by a two-element patch element array. It is shown that beam scanning from $-15°$ to $+15°$ off the broadside direction can be achieved in the frequency range from 5.5 to 5.7 GHz with a maximum gain of 12 dBi. To the best of the authors' knowledge, few solutions can be found in the literature which can realize 3-D beam coverage using reconfigurable FSSs, covering both the azimuth and elevation planes.

Electronic beam tilting has been used in multisector base station antennas to lower intersymbol interference in the network. Much effort has been devoted to developing tilted beam antennas [12]–[15]. Recently, Dadgarpour *et al.* [16] report

Manuscript received July 19, 2016; revised August 16, 2017; accepted August 20, 2017. Date of publication September 28, 2017; date of current version October 27, 2017. This work was supported in part by EPSRC under Grant EP/N032497/1 and in part by the the U.K. Royal Academy of Engineering under Grant ISS1617/48. *(Corresponding author: Chao Gu.)*

C. Gu, S. Gao, B. Sanz-Izquierdo, E. A. Parker, H. Xu, and J. C. Batchelor are with the School of Engineering and Digital Arts, University of Kent, Canterbury CT2 7NT, U.K. (e-mail: c.gu@kent.ac.uk; s.gao@kent.ac.uk).

F. Qin is with the School of Telecommunications Engineering, Xidian University, Xi'an 710071, China.

X. Yang is with the School of Communication Engineering, Shanghai University, Shanghai 200444, China.

Z. Cheng is with the School of Electronic Engineering, Hangzhou Dianzi University, Hangzhou 310018, China.

Color versions of one or more of the figures in this paper are available online at http://ieeexplore.ieee.org.

Digital Object Identifier 10.1109/TAP.2017.2754400

This work is licensed under a Creative Commons Attribution 3.0 License. For more information, see http://creativecommons.org/licenses/by/3.0/

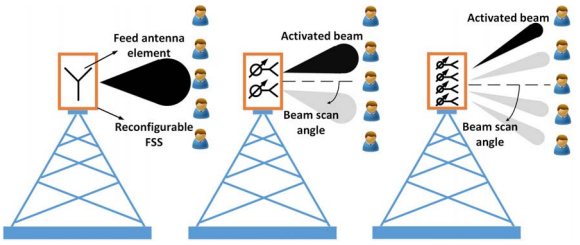

Fig. 1. Proposed antenna application scenario.

a tilted beam technique for planar endfire antennas. Double G-shaped resonator arrays are mounted in the antenna H-plane to create a 35° beam tilt in the elevation plane and a maximum gain enhancement of 5 dB at 3.6 GHz. However, the reported antennas cannot steer the main beam to cover the entire horizontal plane while maintaining the beam tilting in the elevation plane. In this paper, for the first time, we propose a 3-D beam coverage antenna using a reconfigurable cylindrical FSS illuminated by a novel planar feed array. The compact planar array can be easily fabricated and connected to external feed networks to achieve beam scanning in the elevation plane. Based on the study and optimization of the antenna structure that combines the feed array and the active FSS (AFSS) cylinder, the resulting antenna can steer the main beam in both the elevation plane and azimuth plane simultaneously.

II. 3-D Coverage Beam-Scanning Mechanism

The concept of switching the antenna main beam only in the azimuth plane has been demonstrated in [17], where a conventional monopole antenna is explored as the feed. To fulfill beam steering in the elevation plane, we propose a novel collinear feed array excited by progressive phase shifts between elements. Fig. 1 compares different feed schemes inside a reconfigurable FSS cylinder. Increasing the number of elements increase the directivity of the array, and from the beam optimization viewpoint, a larger number of feed elements leads to more freedom to apply sidelobe reduction/beam-shaping techniques to the array.

A. Metallic Reflector Validation

A semicylindrical metallic reflector fed by a dipole is investigated to validate the feasibility of the concept using AFSS [8]. In our design, by exciting each element of the array with specific amplitude and phase, beam scanning in the elevation plane can be achieved. Indeed, the design concept is inspired by a conventional base station antenna design, which consists of incorporate feed dipole array over a planar metallic reflector [18]. Fig. 2 shows a two-element metallic half-wavelength dipole linear array placed along the axis of the semicylindrical reflector whose radius $R = 60$ mm. The length of the reflector is $H = 250$ mm, and the interelement spacing D_e is set to be 70 mm. The simplest method to excite a uniform linear array is to assign the array ports with equal amplitude and a progressive phase shift $\Delta\varphi$. For base station applications, the maximum phase shift is given by the N-element array and the scan angle θ

$$\Delta\varphi_{\max} = -(N-1) \times kd \times \sin\theta \tag{1}$$

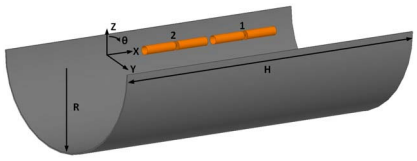

Fig. 2. Schematic view of the two-element fed reflector.

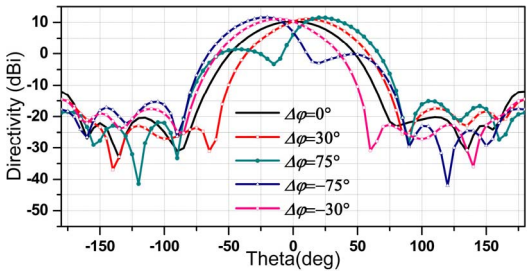

Fig. 3. Two-element array beam scan patterns in the elevation *zox* plane.

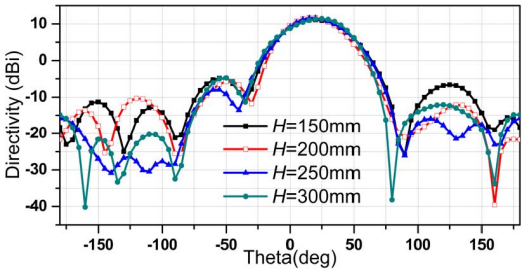

Fig. 4. Effect of reflector length H ($\Delta\varphi = 55°$).

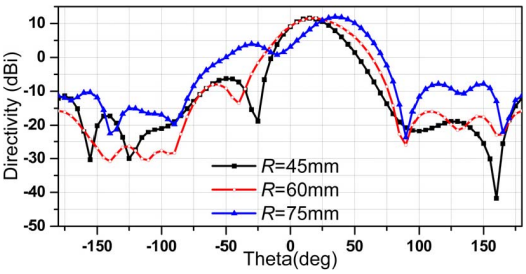

Fig. 5. Effect of reflector radius R($\Delta\varphi = 55°$).

where $k = 2\pi/\lambda$, $d = 0.5\lambda$. The structure in Fig. 2 is simulated in HFSS with lumped ports. Fig. 3 shows that the attainable beam scan range is up to $\pm 25°$ with a maximum sidelobe level (SLL) below -10 dB. The simulated directivity difference across the scan range is less than 2 dB. To optimize the beam tilting performance, three parameters: H, R, and D_e are examined. It is clear from Fig. 4 that the length of the reflector has almost no effect on the antenna directivity, while for the shorter reflectors the SLL is increased by 5 dB. Fig. 5 depicts the effects of the reflector radius. It is noted that larger R leads to extended beam tilt angle at the cost of raised SLL. Finally, Fig. 6 shows that enlarging the spacing between elements just slightly degrades the SLL. Based on the above analysis, the size of the reflector and the element spacing will be used for the following active FSS reflector design.

Next, the scan performance of the four-element array is also carried out with the same R but $H = 320$ mm, as shown

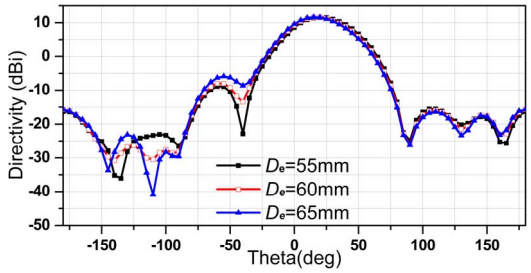

Fig. 6. Effect of array element spacing D_e ($\Delta\varphi = 55°$).

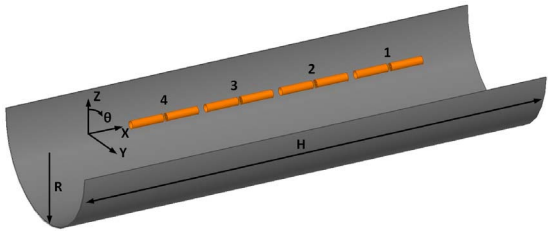

Fig. 7. Schematic view of the four-element fed metallic reflector.

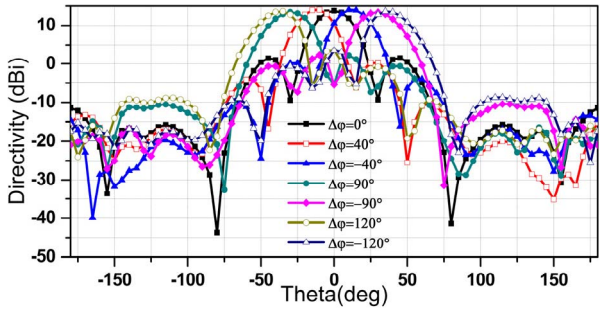

Fig. 8. Four-element array beam scan patterns in the elevation plane.

in Fig. 7. Fig. 8 shows that by applying identical magnitude and phase shift excitation to the four ports, the radiation pattern scans over the range of ±35° with SLLs below −10 dB when the phase difference between the ports is ±120°. Also, the maximum directivity is 14 dBi which is 3 dB larger than the two-element case. Moreover, array synthesis methods can be adopted to provide the desired beam patterns. The most common technique is to introduce an amplitude taper across the array to reduce the SLL, and thus expanding the useful scan angle.

B. AFSS Unit Cell Design

As elaborated in [17], incorporating p-i-n diodes into slot-type FSS elements enables electronic switching of the FSS between reflective or transparent mode. An H-shaped AFSS unit cell based on a switchable slot is designed to operate at 2.45 GHz, as shown in Fig. 9. Similar to a dipole antenna, a slot FSS resonates when the slot length of each element is half wavelength. By Babinet's principle, a slot FSS with slot length S_x embedded in a homogeneous medium characterized by (ε and μ) has a resonance frequency around

$$f_c = \frac{1}{2S_x\sqrt{\varepsilon\mu}}. \tag{2}$$

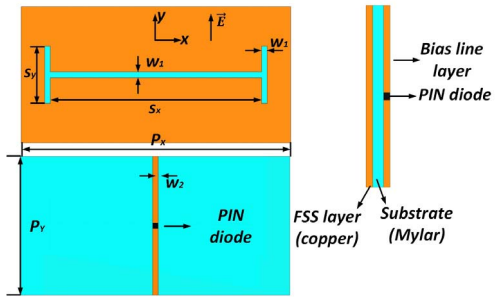

Fig. 9. Schematic view of the unit cell.

TABLE I
UNIT CELL DIMENSIONS [mm]

S_x	S_y	W_1	W_2	P_x	P_y
37	10	1	1	47	23.75

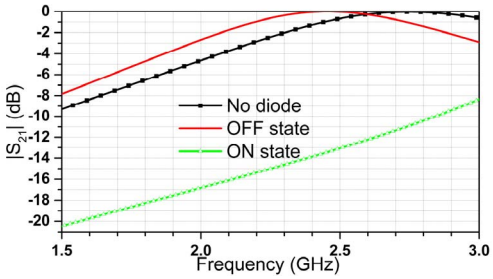

Fig. 10. Simulated AFSS transmission coefficients.

More specifically, with slot width S_y, the resonance frequency can be calculated by

$$f_c = \frac{C}{2.1\left(1 + \frac{S_y}{2S_x}\right)S_x}. \tag{3}$$

In practice, it is difficult to incorporate a p-i-n diode into the single slot FSS copper layer. However, this issue can be addressed by placing the entire p-i-n diode bias network at the other side of the substrate [19]–[21]. Mylar polyester film with $\varepsilon_r = 2.7$, loss tangent of 0.0023, and $h = 0.005$ mm is used as the substrate because: 1) it is flexible, strong, and suitable for conformal antenna design and 2) it has almost no effect on the AFSS performance while the p-i-n diode is located extremely close to the slot. The dimensions of the unit cell are given in Table I. The whole structure is simulated in CST using Floquet mode boundary setup. Specifically, the p-i-n diode ON/OFF states are modeled as series or parallel *RLC* lumped elements. For the ON state, the diode is simplified as a forward resistor $R_s = 2.1\ \Omega$, and as an equivalent capacitor, $C_s = 0.17$ pF in the OFF state. Note that the H-shaped slot can reduce the FSS array periodicity P_x, enabling accommodation of more cells for a fixed cylinder perimeter. Compared with the dimension in [17], the diameter of the AFSS cylinder consisting of H-shaped unit cells can reduce by one effective wavelength size.

The simulated transmission coefficients of the AFSS are shown in Fig. 10. It is found that by inserting an OFF-state

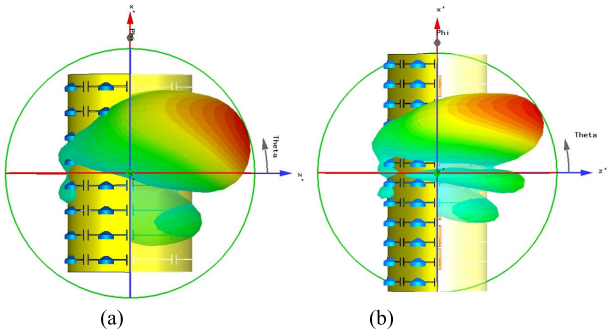

Fig. 11. Up tilted beam states fed by (a) two-element array and (b) four-element array.

diode into the gap of the bias line, a capacitance is introduced which shifts the resonance frequency from 2.75 to 2.45 GHz. The simulated ON-state frequency response exhibits about −14 dB transmission magnitude, which indicates about 96% EM wave energy has been reflected. Thus, by switching the p-i-n diodes, the AFSS can be reconfigured as an EM transparent window or a reflector.

C. Array Fed AFSS Cylinder Validation

To imitate the radiating mechanism of a corner reflector antenna in Fig. 2, the planar AFSS was rolled into a cylinder which has the same dimensions of the metallic reflector. First, the numbers of the unit cells along the circumference and axis: N_x and N_y can be calculated from $N_x = 2 \times \pi R/P_x$ and $N_y = L/P_y$, where $R = 60$ mm and $L = 190$ mm. Next, the same linear arrays feeding the metallic reflector cases in Section II-A are employed to illuminate the AFSS reflector. Note that the more unit cells along the cylinder circumference, the more beams that can be generated in the horizontal plane. The whole antenna configuration was simulated using CST frequency-domain solver. Fig. 11 shows the radiation patterns of the AFSS cylinder fed by two- and four-element arrays. In Fig. 11(a), the cylindrical AFSS consists of eight columns and eight rows of unit cells whose dimensions are given in Table I. The p-i-n diodes in the left-half cylinder are switched ON to activate the reflecting mode of the left-half AFSS, whereas the other half diodes are all OFF, which allows the EM wave to pass through the right-half cylinder (half of the AFSS has been made transparent for clarity). By varying the phase shifts applied to the array element ports, similar beam tilting trends can be obtained. The maximum beam tilt angle with an SLL of −10 dB is reduced to ±21°, as shown in Fig. 12. Because the AFSS cannot absolutely replace the metallic reflector, the directivities of the scanned beams are slightly lower than the ones in Fig. 3. Fig. 13 shows the steered E-plane radiation patterns of the four-element array fed AFSS cylinder which consists of 8 columns and 12 rows shown in Fig. 11(b). It can be seen that the maximum beam scan angle is ±30°, which is 5° less than the one in Fig. 8.

III. Feed Array Design

In this section, a multilayer omnidirectional antenna array with corresponding power distribution networks is proposed to replace the ideal collinear dipole array in Section II.

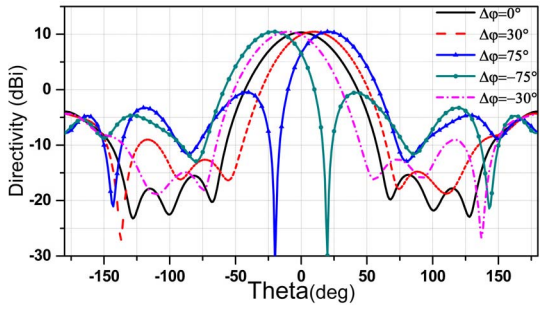

Fig. 12. Scanned radiation patterns in the elevation plane (two element).

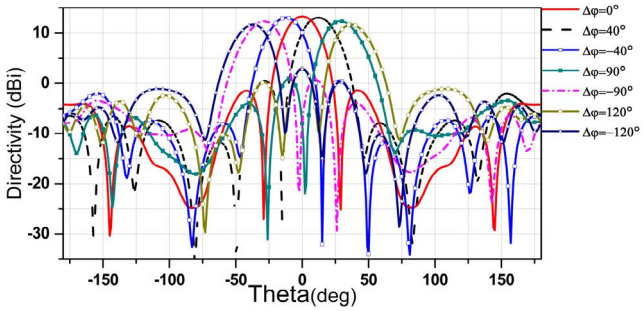

Fig. 13. Scanned radiation patterns in the elevation plane (four element).

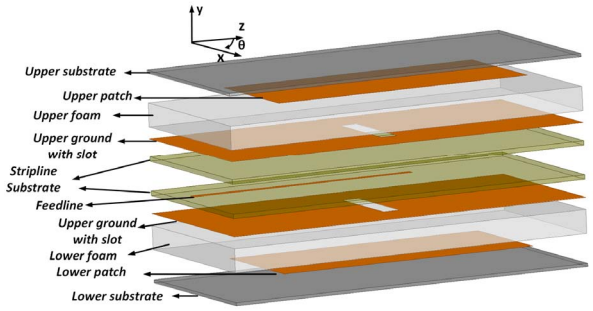

Fig. 14. Schematic view of the array element.

A. Antenna Feed Array Element

It is desired that omnidirectional antenna elements should be fed collinearly and placed axially inside the AFSS cylinder. In [22], a simple stripline structure is introduced to serially feed loop slots etched on each metal ground. As described in [23] and [24], significantly reducing the size of the ground plane makes the H-plane pattern of the antenna nearly omnidirectional. Thus by arranging two identical rectangular patches back-to-back along the broadside direction, the radiated far field of the two elements is added to form an omnidirectional pattern in the azimuth plane. As shown in Fig. 14, the multilayered element consists of two identical patches, which are fed by a stripline through the two slots in the ground plane. The rectangular patches are etched on Arlon Cuclad 217 ($\varepsilon_r = 2.17$ and loss tangent $= 0.0009$) with a thickness of 0.508 mm. Because the substrate is quite flexible, two pieces of ROHACELL foams are used as the spacer to support the patches. The substrate used for the stripline is 0.762 mm thick Arlon AD255A whose ε_r is 2.55 and loss tangent is 0.0015.

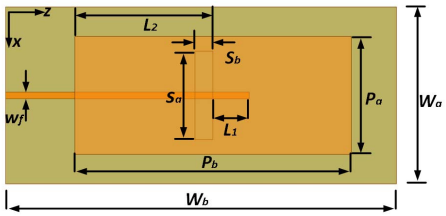

Fig. 15. Top view of the element.

TABLE II
ARRAY ELEMENT DIMENSIONS [mm]

W_a	W_b	P_a	P_b	S_a	S_b
30	65	20	46	15	3
W_f	L_1	L_2			
1.1	6	20			

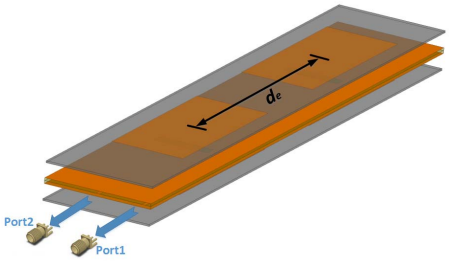

Fig. 16. Perspective view of the feed array.

Fig. 17. Details of the feedlines.

Fig. 15 shows the top view of the element whose dimensions are given in Table II. It should be noted that if a harder substrate is used, this design does not require any foam layer as nylon screws can be used to fix the patch layers.

B. Antenna Feed Array Design

Using the above element, a two-element parallel fed array is designed and experimentally tested. Fig. 16 depicts the configuration of the array antenna which consists of two elements with a center-to-center spacing d_e. The feeding points at the bottom can be connected to phase shifters and feed networks through stripline to coaxial/microstrip line transition. To avoid grating lobes, the element spacing d_e is kept around 0.5–0.7λ in the substrate at the desired frequency. Fig. 17 shows the detailed feedline layout of the stripline. In order to maintain a good isolation between the two elements, the feedline of the upper element is offset some distance f_2 from the coupling slot of the lower element as far as possible. The stripline is designed to have a 50 Ω characteristic impedance. Table III presents the parameters of the array design. One profound advantage of this design over the conventional metallic collinear dipole array is the feedlines hidden between the grounds, which allow one of the feedlines to pass through the lower element without affecting its performance. The simulated S-parameters are presented in Fig. 18. It can be observed that with respect to below −10 dB S_{11}, the antenna array covers the frequency bands from 2.51 to 2.62 GHz (S_{11} will shift toward lower frequency when integrating with AFSS). Moreover, the isolation between two ports is larger than 25 dB.

TABLE III
ARRAY DESIGN PARAMETERS [mm]

d_e	f_1	f_2	f_3	f_4
70	6.5	13	109	45

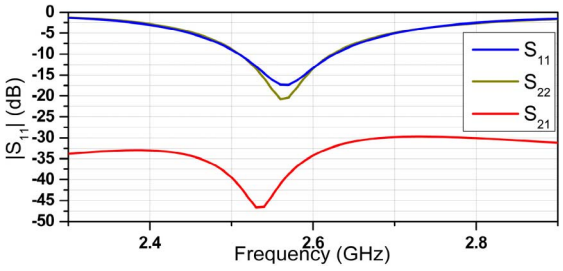

Fig. 18. Simulated S-parameters of the array.

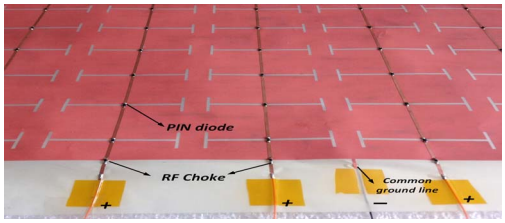

Fig. 19. Detailed bias network design.

IV. AFSS ANTENNA DESIGN, FABRICATION, AND MEASUREMENT

To integrate the AFSS and the feed array, measurements were carried out to ensure the performance of the final structure. First, the transmission coefficients of the proposed planar AFSS in Section II were measured in a plane wave chamber, where two wideband log-periodic antennas are used as the transmitting and receiving antennas. The flat AFSS sheet is comprised of 8 × 8 unit cells with dimensions in Fig. 9 and Table I and fixed in a support between the two antennas. Fig. 19 shows the fabricated FSS and its bias network. Eight parallel lines with p-i-n diodes in series are etched on one side of the substrate whereas, on the other side is the copper layer with FSS slots which is used as the common ground for the lines through a metallic via. Thus, it is convenient to control each column with a 5 V dc voltage and there is only one line connected to the ground. RF inductors are selected as chokes to isolate the RF signal

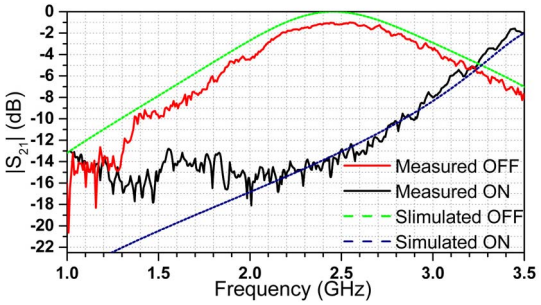

Fig. 20. Measured and simulated AFSS transmission coefficients.

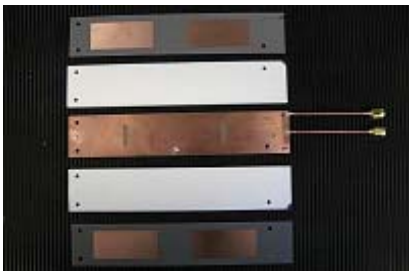

Fig. 21. Fabricated feed array before assembling.

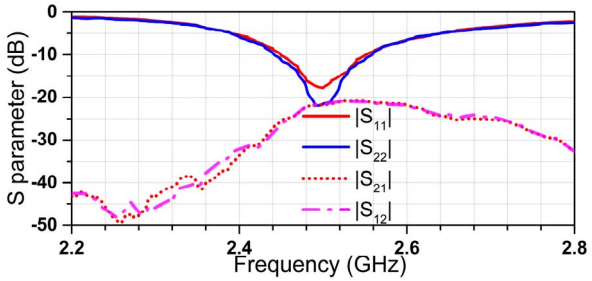

Fig. 22. Measured *S*-parameters of the array.

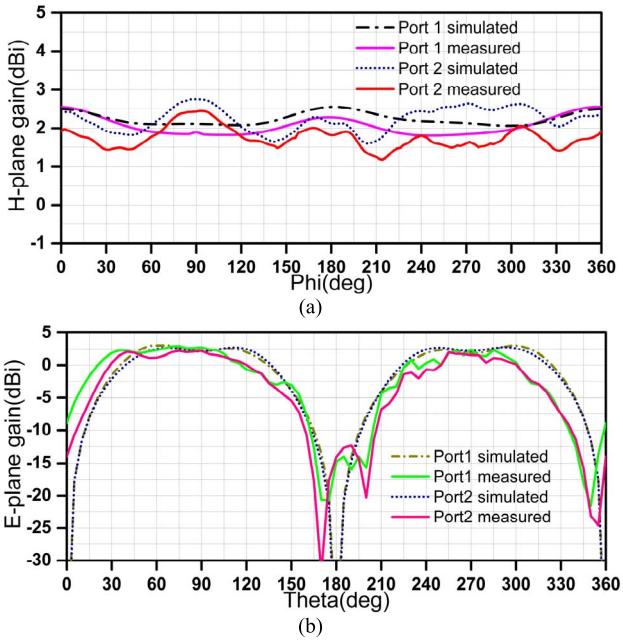

Fig. 23. (a) Simulated and (b) measured radiation patterns of the two ports.

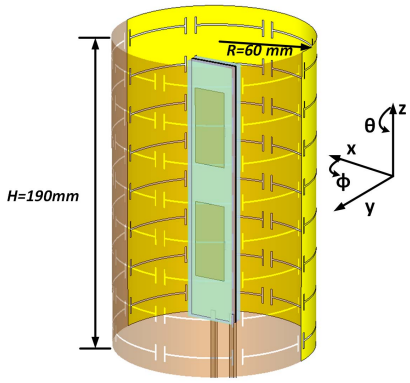

Fig. 24. Perspective view of the final antenna.

and a 1 kΩ resistor is added to the ground line to limit the current. Fig. 20 compares the simulated and measured values of S_{21} when switching ON/OFF all the p-i-n diodes. It can be noted that the performance of the fabricated planar AFSS agrees well with the simulated one except that there is 1 dB transmission loss at the resonant frequency.

Next, the feed array with the dimensions in Tables II and III was fabricated, as shown in Fig. 21. Fig. 22 shows the measured *S*-parameters. It is clear that the S_{11} and S_{21} follow the same trend as the simulated results in Fig. 18. However, the measured port isolation is less than the predicted results but still larger than 20 dB which is sufficient for most cases. Two coaxial cables are connected to the feed ports of the two antenna elements, which are also for attaching external power combining networks with required phase shifts. Fig. 23 illustrates the measured radiation patterns of the two array ports. As can been seen from the H-plane results, omnidirectional patterns (deviation from omni $\leq$ 1.5 dBi) can be achieved using the presented antenna elements.

The final stage is to combine the cylindrical AFSS and the feed array. To fully investigate the antenna characteristics, the entire structure in Fig. 24 is simulated in CST using the frequency-domain solver. Note that all the p-i-n diodes in the gaps of the slots are omitted for clarity. The feed array is placed in the center of the cylinder parallel to the *xoz* plane. The bottom two feed points are extended beyond the cylinder to connect the feed network circuits. Within this configuration, where the solid sector (yellow) acts as a reflector by switching ON all the diodes in it, the phase shifts required are obtained by optimizing the progressive phase difference and element spacing in the simulation. Then, the attained phase shifts are applied to the microstrip lines of the feed network, allowing the array pattern tilted to the desired angle.

Fig. 25 compares the simulated and measured *S*-parameters of the array fed AFSS antenna. It is clear that the resulting antenna has a below -10 dB S_{11} bandwidth covering 2.4–2.5 GHz. Meanwhile, the isolation of the two ports is found to be reduced to around 14 dB due to the presence of the AFSS cylinder. To compensate this adverse effect, the coupling between the antenna elements and the single-element reflection

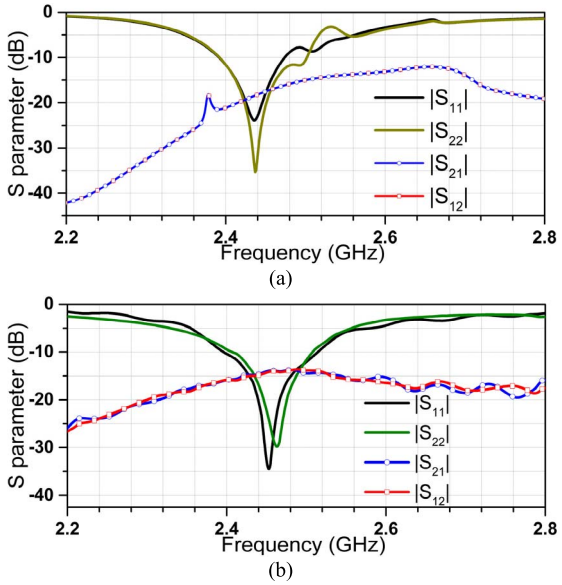

Fig. 25. (a) Simulated and (b) measured S-parameters of the AFSS antenna.

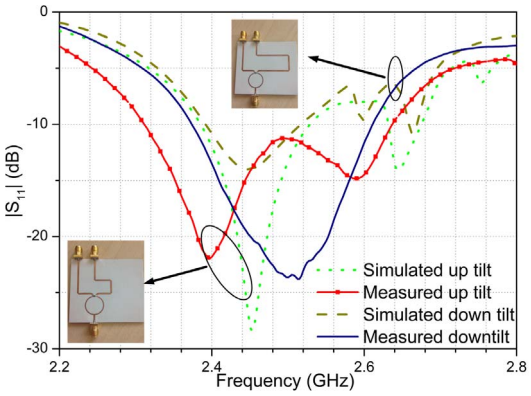

Fig. 26. Simulated and measured S_{11} of the AFSS antenna with feed network.

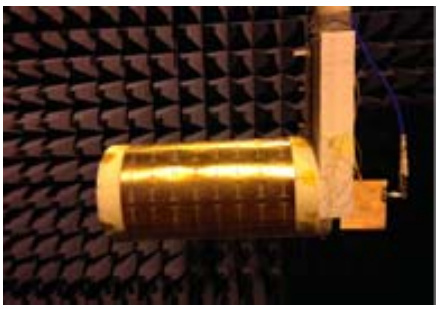

Fig. 27. Fabricated antenna under test.

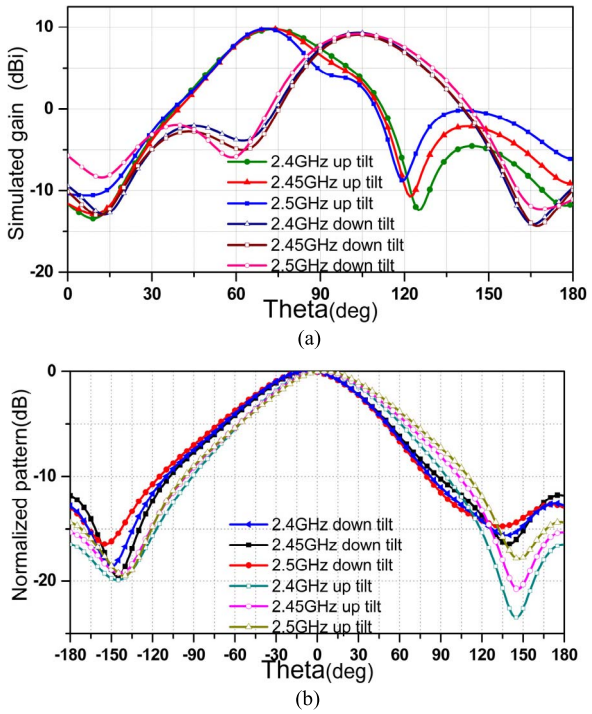

Fig. 28. Simulated (a) E-plane and (b) H-plane radiation patterns.

coefficient has to be kept as low as possible in order to allow an independent design of the array feed distribution and the feed network. The array element spacing is a key parameter to tune the coupling, but it also affects the beam scan angle and SLL. According to the simulated results, the required phase shifts for the up and down tilt beams are 45° and 245°, respectively, when the beams are pointed at ±15°, with maximum −10 dB SLLs. Thus two individual feed network circuits including the required phase shift values are simulated with the structure in Fig. 24. In Fig. 26, the simulated and measured reflection coefficients of the final structure with external feed networks are compared. For the two tilt angles, both designs can satisfy the 2.45 GHz WIFI frequency band. The fabricated antenna under test is shown in Fig. 27. The feed array is inserted into a hollowed cylindrical foam, which supports the AFSS. The whole structure is supported in turn by a vertical section of foam, to minimize scattering.

The beam tilting performance of the proposed antenna was experimentally validated in an anechoic chamber. Figs. 28 and 29 show the comparison between the simulated radiation patterns and the measured ones in the E-plane and H-plane. In Fig. 28(a), the simulated up and down tilt angles are 73° and 105°, respectively, with below −10 dB SLLs. Fig. 29(a) shows the measured up tilt angle has a 2° decrease over the operating frequencies from 2.4 to 2.5 GHz but a 3 dB lower SLL at 2.5 GHz. The measured down tilt scan angles are 2° larger than the simulated ones at 2.45 and 2.5 GHz. Also, there is a slight rise in SLL for the down tilt beam at 2.5 GHz. Note that for the measurements, a half sector is biased to act as a reflector. It is expected that eight identical up/down beams can be generated if we switch ON/OFF half of the AFSS cylinder in turn due to the symmetry of the antenna structure. Compared with the simulated results of the array fed metallic reflector, the scan angle for the same SLL (−10 dB) is reduced mainly because the AFSS is not ideal as a conventional reflector. Furthermore, unwanted scattering happens when EM waves pass through the OFF-state AFSS, which degrades the beam tilting performance as well. Fig. 30 shows the measured eight beams in the horizontal plane for the up and down tilt angles at 2.45 GHz.

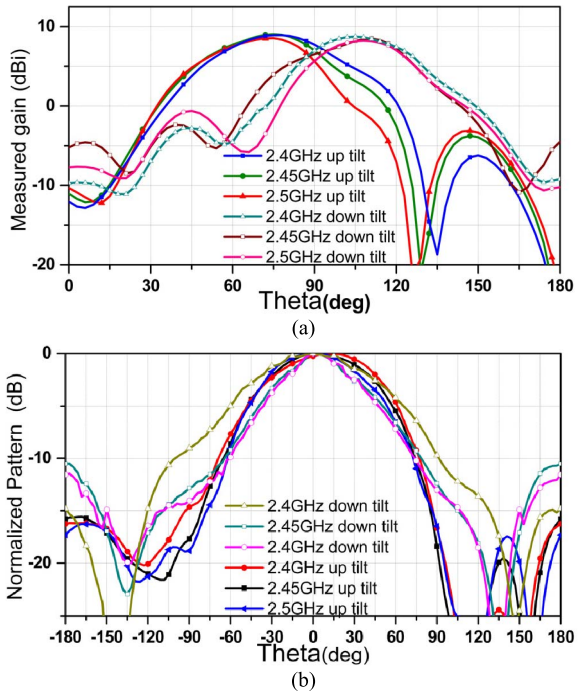

Fig. 29. Measured (a) E-plane and (b) H-plane radiation patterns.

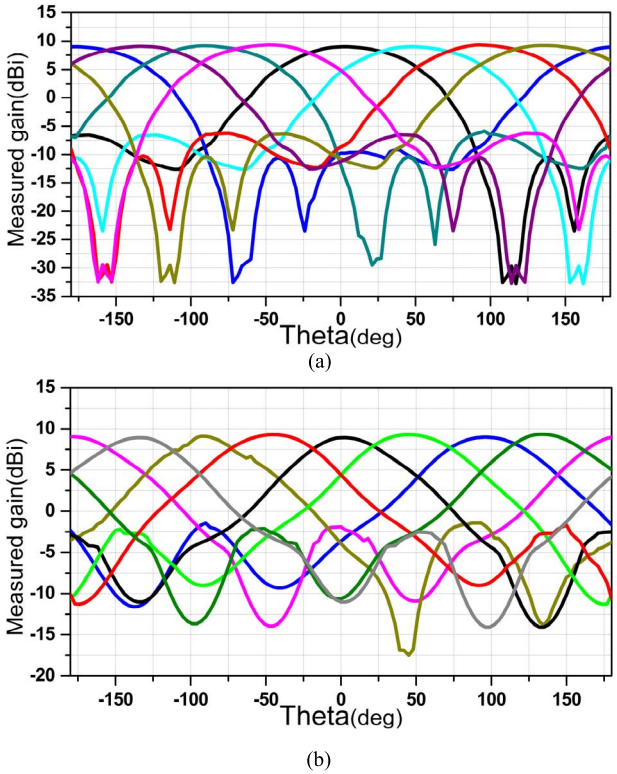

Fig. 30. Measured (a) up tilt and (b) down tilt radiation pattern switching in the horizontal plane.

Table IV compares the characteristics between several beam-switching antennas recently reported and our design. It can be seen that the proposed antenna has the advantages of being able to achieve beam scanning in both the horizontal and elevation planes with a moderate gain. In addition, the dimensions of our antenna are smaller than the ones in [17] which also uses a slot-type active FSS cylinder.

TABLE IV
COMPARISON OF THE PROPOSED ANTENNA WITH PREVIOUS WORKS

Ref No.	[11]	[12]	[14]	[17]	This work
Beam scan mode	1D	1D	1D	2D	3D
Broadside	±15°	No	No	No	No
Elevation plane	No	9°	28°	No	+16°/ -15°
Horizontal plane	No	No	No	360° coverage	360° coverage
Gain (dBi)	12	8.3	11*	8.7	9.2
Max. SLL (dB)	-9	-12	-5	-5	-9
Dimensions	2.2λ ×2.2λ ×0.5λ	2.2λ×2λ (planar)	2.6λ×0.6 λ ×0.6λ	1.8λ ×1.8λ ×1.63λ	1λ ×1λ ×1.55λ

*11dBi is the measured directivity given in Ref [14].

V. CONCLUSION

Low-cost smart antennas are important for a wide range of applications in wireless communications. This paper presents the first report of a 3-D coverage beam-scanning antenna utilizing an active FSS. A prototype at 2.45 GHz has been designed, fabricated, and measured to verify the design principles. In the azimuth plane, the proposed antenna is shown to be able to achieve electronically beam switching covering a full 360° range. In the elevation plane, the antenna achieves a scan range of $+16°/-15°$. A measured maximum gain of 9.2 dBi is obtained and the antenna is scalable to achieve a higher gain. Compared with traditional smart antennas, this antenna does not require a large number of microwave phase shifters, has a simple structure and low cost, and thus is promising for base station applications in wireless communications.

REFERENCES

[1] W. A. Imbriale, S. Gao, and L. Boccia, *Space Antenna Handbook*. New York, NY, USA: Wiley, 2012.
[2] A. Sibille and S. Fassetta, "Intersector correlations: A quantitative approach to switched beams' diversity performance in wireless communications," *IEEE Trans. Antennas Propag.*, vol. 51, no. 9, pp. 2238–2243, Sep. 2003.
[3] J. D. Boerman and J. T. Bernhard, "Performance study of pattern reconfigurable antennas in MIMO communication systems," *IEEE Trans. Antennas Propag.*, vol. 56, no. 1, pp. 231–236, Jan. 2008.
[4] C. Gu *et al.*, "Compact smart antenna with electronic beam-switching and reconfigurable polarizations," *IEEE Trans. Antennas Propag.*, vol. 63, no. 12, pp. 5325–5333, Dec. 2015.
[5] H.-T. Liu, S. Gao, and T.-H. Loh, "Electrically small and low cost smart antenna for wireless communication," *IEEE Trans. Antennas Propag.*, vol. 60, no. 3, pp. 1540–1549, Mar. 2012.
[6] D. Rodrigo, L. Jofre, and B. A. Cetiner, "Circular beam-steering reconfigurable antenna with liquid metal parasitics," *IEEE Trans. Antennas Propag.*, vol. 60, no. 4, pp. 1796–1802, Apr. 2012.
[7] M. Niroo-Jazi and T. A. Denidni, "Electronically sweeping-beam antenna using a new cylindrical frequency-selective surface," *IEEE Trans. Antennas Propag.*, vol. 61, no. 2, pp. 666–676, Feb. 2013.
[8] A. Edalati and T. A. Denidni, "High-gain reconfigurable sectoral antenna using an active cylindrical FSS structure," *IEEE Trans. Antennas Propag.*, vol. 59, no. 7, pp. 2464–2472, Jul. 2011.

[9] A. Edalati and T. A. Denidni, "Frequency selective surfaces for beam-switching applications," *IEEE Trans. Antennas Propag.*, vol. 61, no. 1, pp. 195–200, Jan. 2013.
[10] C. Gu *et al.*, "Dual-band electronically beam-switched antenna using slot active frequency selective surface," *IEEE Trans. Antennas Propag.*, vol. 65, no. 3, pp. 1393–1398, Mar. 2017.
[11] L. Y. Ji, Y. J. Guo, P. Y. Qin, S. X. Gong, and R. Mittra, "A reconfigurable partially reflective surface (PRS) antenna for beam steering," *IEEE Trans. Antennas Propag.*, vol. 63, no. 6, pp. 2387–2395, Jun. 2015.
[12] C.-H. Ko, K. M. J. Ho, and G. M. Rebeiz, "An electronically-scanned 1.8–2.1 GHz base-station antenna using packaged high-reliability RF MEMS phase shifters," *IEEE Trans. Microw. Theory Techn.*, vol. 61, no. 2, pp. 979–985, Feb. 2013.
[13] M. Li, S.-Q. Xiao, Z. Wang, and B.-Z. Wang, "Compact surface-wave assisted beam-steerable antenna based on HIS," *IEEE Trans. Antennas Propag.*, vol. 62, no. 7, pp. 3511–3519, Jul. 2014.
[14] I. Kim and Y. Rahmat-Samii, "Electromagnetic band gap-dipole sub-array antennas creating an enhanced tilted beams for future base station," *IET Microw., Antennas Propag.*, vol. 9, no. 4, pp. 319–327, Mar. 2015.
[15] R. B. Hwang, Y. J. Chang, and M.-I. Lai, "A low-cost electrical beam tilting base station antennas for wireless communication system," *IEEE Trans. Antennas Propag.*, vol. 52, no. 1, pp. 115–121, Jan. 2004.
[16] A. Dadgarpour, B. Zarghooni, B. S. Virdee, and T. A. Denidni, "Enhancement of tilted beam in elevation plane for planar end-fire antennas using artificial dielectric medium," *IEEE Trans. Antennas Propag.*, vol. 63, no. 10, pp. 4540–4545, Oct. 2015.
[17] B. Liang, B. Sanz-Izquierdo, E. A. Parker, and J. C. Batchelor, "Cylindrical slot FSS configuration for beam-switching applications," *IEEE Trans. Antennas Propag.*, vol. 63, no. 1, pp. 166–173, Jan. 2015.
[18] Z. Zaharis, E. Vafiadis, and J. N. Sahalos, "On the design of a dual-band base station wire antenna," *IEEE Antennas Propag. Mag.*, vol. 42, no. 6, pp. 144–151, Dec. 2000.
[19] B. Sanz-Izquierdo, E. A. Parker, J.-B. Robertson, and J. C. Batchelor, "Tuning technique for active FSS arrays," *Electron. Lett.*, vol. 45, no. 22, pp. 1107–1109, Oct. 2009.
[20] B. Sanz-Izquierdo, E. A. Parker, and J. C. Batchelor, "Dual-band tunable screen using complementary split ring resonators," *IEEE Trans. Antennas Propag.*, vol. 58, no. 11, pp. 3761–3765, Nov. 2010.
[21] B. Sanz-Izquierdo, E. A. Parker, and J. C. Batchelor, "Switchable frequency selective slot arrays," *IEEE Trans. Antennas Propag.*, vol. 59, no. 7, pp. 2728–2731, Jul. 2011.
[22] X. Chen, K. Huang, and X.-B. Xu, "A novel planar slot array antenna with omnidirectional pattern," *IEEE Trans. Antennas Propag.*, vol. 59, no. 12, pp. 4853–4857, Dec. 2011.
[23] K. Ogawa and T. Uwano, "A variable tilted fan beam antenna for indoor base stations," in *IEEE Int. Symp. Dig. Antennas Propag.*, Jun. 1994, pp. 332–335.
[24] S.-W. Lu, T.-F. Huang, and P. Hsu, "CPW-fed slot-loop coupled patch antenna on narrow substrate," *Electron. Lett.*, vol. 35, no. 9, pp. 682–683, Apr. 1999.

Chao Gu received the B.S and M.S. degrees from Xidian University, Xi'an, China, in 2009 and 2012, respectively, and the Ph.D. degree from the University of Kent, Canterbury, U.K., in 2017.

Steven (Shichang) Gao (SM'16) is a Professor and Chair in RF and Microwave Engineering with the University of Kent, Canterbury, U.K.

Benito Sanz-Izquierdo is a Lecturer in electronic systems with the University of Kent, Canterbury, U.K.

Edward A. Parker is an Emeritus Professor of radio communications with the University of Kent, Canterbury, U.K.

Fan Qin, photograph and biography not available at the time of publication.

Hang Xu, photograph and biography not available at the time of publication.

John C. Batchelor, photograph and biography not available at the time of publication.

Xuexia Yang, photograph and biography not available at the time of publication.

Zhiqun Cheng, photograph and biography not available at the time of publication.